Structural transition and amorphization in compressed α-Sb$_2$O$_3$

Zhao Zhao,[1,2,*] Qiaoshi Zeng,[2,3,4] Haijun Zhang,[5,1] Shibing Wang,[2,3] Shigeto Hirai,[2,3]
Zhidan Zeng,[2,3,4] and Wendy L. Mao[2,3]

[1]*Department of Physics, Stanford University, Stanford, California 94305, USA*
[2]*Stanford Institute for Materials and Energy Sciences, SLAC National Accelerator Laboratory, Menlo Park, California 94025, USA*
[3]*Department of Geological Sciences, Stanford University, Stanford, California 94305, USA*
[4]*Center for High Pressure Science and Technology Advanced Research, Shanghai 201203, China*
[5]*National Laboratory of Solid State Microstructures, School of Physics, Collaborative Innovation Center of Advanced Microstructures,
Nanjing University, Nanjing 210093, China*

Sb$_2$O$_3$-based materials are of broad interest in materials science and industry. High-pressure study using diamond anvil cells shows promise in obtaining new crystal and electronic structures different from their pristine states. Here, we conducted *in situ* angle dispersive synchrotron x-ray-diffraction and Raman spectroscopy experiments on α-Sb$_2$O$_3$ up to 50 GPa with neon as the pressure transmitting medium. A first-order structural transition was observed in between 15 and 20 GPa, where the cubic phase I gradually transformed into a layered tetragonal phase II through structural distortion and symmetry breaking. To explain the dramatic changes in sample color and transparency, we performed first-principles calculations to track the evolution of its density of states and electronic structure under pressure. At higher pressure, a sluggish amorphization was observed. Our results highlight the structural connections among the sesquioxides, where the lone electron pair plays an important role in determining the local structures.

I. INTRODUCTION

Sb$_2$O$_3$-based materials are of broad interest in materials science and industry [1–24]. Because of their unique mechanical, chemical, and electronic properties, they are applicable as flame retardants for ceramics and fibers [12] and can be fabricated into nonlinear optical devices [13,25]. Sb$_2$O$_3$ belongs to the late XV group sesquioxides which also include As$_2$O$_3$ and Bi$_2$O$_3$. Various polymorphs have been identified among sesquioxides [4,7,8,10,26–33]. For Sb$_2$O$_3$, three polymorphs α-Sb$_2$O$_3$ (senarmontite) [4,7,8,10], β-Sb$_2$O$_3$ (valentinite) [7], and γ-Sb$_2$O$_3$ [34] have been reported. Cubic α-Sb$_2$O$_3$ (space group *Fd-3m*) is the stable form at ambient pressure and temperature below 570 °C, and it can be viewed as a molecular crystal composed of Sb$_4$O$_6$ adamantanoid cages [see Fig. 1(a)] [4,7,8,10,35,36]. Orthorhombic β-Sb$_2$O$_3$ (space group *Pccn*) becomes more stable at ambient pressure and temperature above 570 °C up to the melting point, and it is composed of membrane rings built by SbO$_3$ pyramids [7]. γ-Sb$_2$O$_3$ is a quenchable (to ambient conditions) phase synthesized at high temperature (300 to 500 °C) and high pressure (9–11 GPa), and this structure [see Fig. 1(d)] is constructed by cross linked Sb-O$_4$ units [34].

Close structural connections exist among late XV group sesquioxides. For example, *c*-As$_2$O$_3$(arsenolite) has a similar structure to α-Sb$_2$O$_3$, and β-Sb$_2$O$_3$ is isostructural to ε-Bi$_2$O$_3$ [4,6–8,10,37–40]. Interestingly, recent theoretical studies showed that many structures such as α-Sb$_2$O$_3$, β-Sb$_2$O$_3$, and β-Bi$_2$O$_3$ could be derived from a defective fluorite structure through symmetry breakings and local distortions [19,41]. Pressure is a powerful tool in tuning the atomic distances and arrangements, and thus may enable studies on the connections between these structural models.

Previous studies have identified a number of pressure-induced structural transitions and amorphization in Bi$_2$O$_3$, Sb$_2$O$_3$ and As$_2$O$_3$ [18,20,34,41–48]. For α-Sb$_2$O$_3$, a high-pressure study combing x-ray diffraction (XRD) and Raman experiments with *ab initio* calculations [20] reported several interesting results. It demonstrated that two isostructural transitions occurred at 3.5 and 10 GPa. Furthermore, it suggested that α-Sb$_2$O$_3$ would transform into a tetragonal structure above 25 GPa [20]. However, this transition was not verified by their experiments due to a lack of pressure. Therefore, experiments at higher pressure are required to study potential phase transitions in α-Sb$_2$O$_3$ and explore the relationship among different structures in XV group sesquioxides.

In this work, we conducted *in situ* XRD and Raman spectroscopy measurements to ~50 GPa on α-Sb$_2$O$_3$ with neon as the pressure medium. We identified a first-order structural transition from the initial cubic structure to a tetragonal structure at ~15 GPa and further discovered an amorphous phase at higher pressure. In addition, we performed *ab initio* calculations on the electronic states of the two phases and the results shed light on the as-observed sharp changes in sample transparency under pressure.

II. EXPERIMENTAL AND THEORETICAL METHODS

Near stoichiometric (purity greater than 99%) cubic α-Sb$_2$O$_3$ powder was purchased from Sigma-Aldrich Product No. 230898 and Lot No. MKBJ9063. Symmetric diamond anvil cells (DACs) with 300-μm culets size were used to generate high pressure. Tungsten gaskets were pre-indented to 20 GPa and a 150-μm-diameter sample chamber was drilled in the center of the indent. *In situ* angle dispersive XRD data were collected
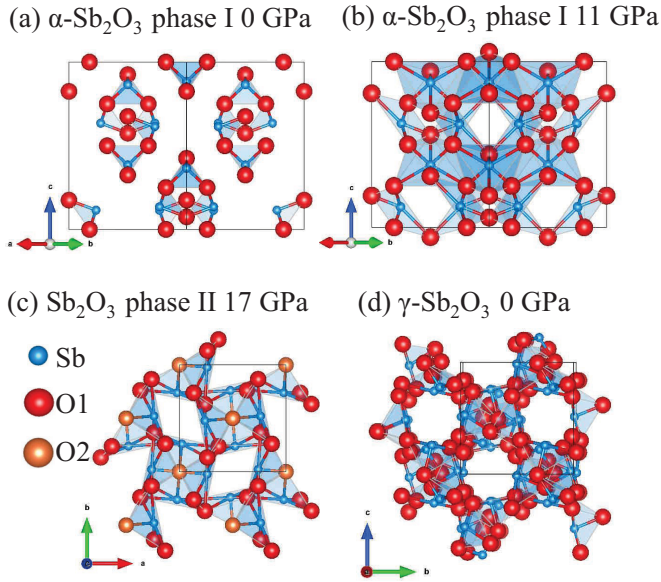
———————
*zhaozhao@stanford.edu

FIG. 1. (Color online) Structures of (a) α-Sb$_2$O$_3$ phase I at ambient conditions, (b) α-Sb$_2$O$_3$ phase I at 11 GPa, (c) Sb$_2$O$_3$ tetragonal phase II at 17 GPa, with two O sites (d) γ-Sb$_2$O$_3$ at ambient conditions, from Ref. [34], where there are six O sites.

at beamline 16 BM-D of the Advanced Photon Source (APS), Argonne National Laboratory (ANL), and at beamline 12.2.2 of the Advanced Light Source (ALS), Lawrence Berkeley National Laboratory (LBNL). The x-ray wavelength was 0.4246 Å. The Rietveld refinement of the integrated powder-diffraction patterns was performed using the GSAS-EXPGUI package [49]. Raman spectra were collected using a Renishaw inVia micro-Raman system with a 514-nm laser excitation line in the Extreme Environments Laboratory, Stanford University. Neon was used as the pressure transmitting medium for both the XRD and Raman measurements. Gas loading was performed at GSECARS, APS, ANL, and the Extreme Environments Laboratory.

For the first-principles calculations, the Vienna *ab initio* Simulation Package (VASP) [50,51] was employed with the framework of Perdew-Burke-Ernzerhof-type [52] generalized gradient approximation of density functional theory [53]. The projector augmented wave [54] pseudopotential was used for all the calculations. The kinetic-energy cutoff was fixed at 450 eV. The lattice parameters were directly taken from the Rietveld refinement. The theoretical atomic positions are electronically relaxed based on the experimental atomic positions.

III. RESULTS AND DISCUSSION

A. *In situ* x-ray-diffraction experiments

Experimental XRD patterns are shown in Fig. 2(a). A first-order structural transition from cubic phase I to tetragonal phase II occurred at ~15 GPa, where the cubic structure could not fit higher pressure patterns. This transition was characterized by the asymmetric broadening of phase I's peaks. The largest d-spacing (111) reflection from phase I
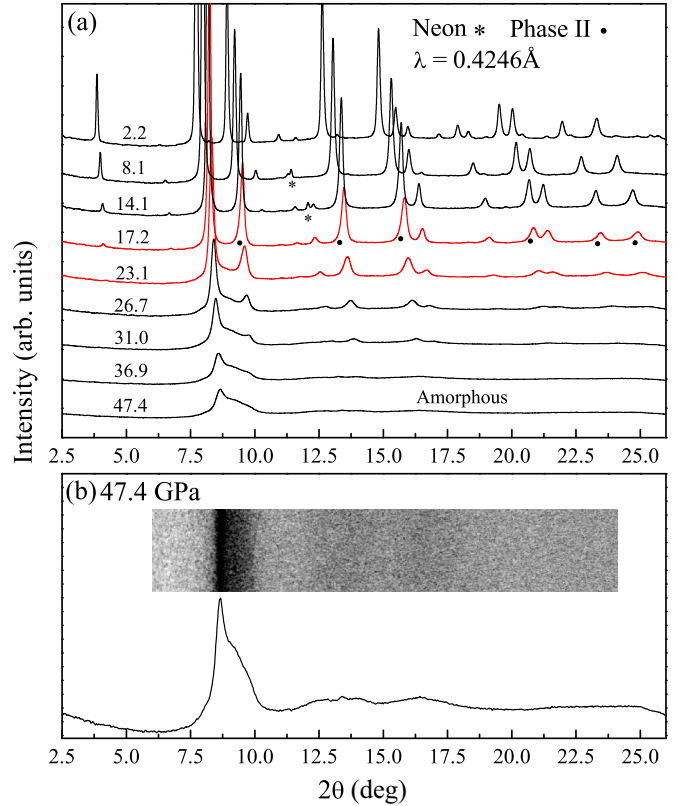

FIG. 2. (Color online) (a) Representative XRD patterns collected during compression up to 47.4 GPa with x-ray wavelength of 0.4246 Å. The numbers represent pressures in unit of GPa. (b) XRD pattern at the highest pressure shows the lack of long-range order; inset is the cake two-dimensional (2D) image.

disappeared completely when the transition was complete at ~20 GPa. At pressure higher than 25 GPa, the sample started to lose its long-range order and an amorphous component was observed [Fig. 2(b)]. Decompression experiment show that the amorphous component is quenchable and the details will be presented elsewhere.

At ambient pressure, the unit-cell volume we measured was 1383.5(1) Å^3, agreeing well with previous data [7,20]. The volume as a function of pressure is presented in Fig. 3. The Fig. 3 inset shows the evolution of the cell parameters under pressure. The cell parameters a and c in the tetragonal phase II (4 Sb$_2$O$_3$ per unit cell) are multiplied by different factors to match the unit-cell volume of cubic phase I (16 Sb$_2$O$_3$ per unit cell). In the previous study, the (111) reflection disappeared completely at 17.9 GPa, and the (400) became much broader being in fact composed of two close peaks (002) and (220) from phase II; see Fig. 4(b). It is worth noting that its calculated volume is quite different from our experimental data, off by 2% to 3%; see Fig. 3. The different enthalpies from experimental volumes and theoretical volumes may explain why the first-order structural transition occurred at a lower pressure experimentally (15–20 GPa) than predicted (i.e., above 25 GPa) [20]. Also, there may lie a region where phase I and phase II coexist.
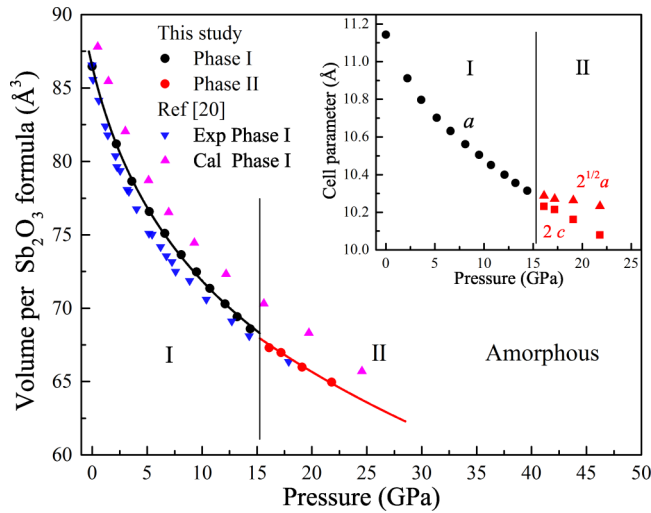
FIG. 3. (Color online) Pressure vs volume for Sb_2O_3. Phase I is shown in black and phase II in red. The inset shows the evolution of cell parameters under pressure. The cell parameters a and c in tetragonal phase II (4 Sb_2O_3 per unit cell) are multiplied by different factors to match the unit-cell volume of cubic phase I (16 Sb_2O_3 per unit cell).

For phase I, we fit our data to a third-order Birch-Murnaghan equation of state (BM-EOS) with fixed experimental $V_0 = 86.47(1)$ Å^3 per formula, and obtained $B_0 = 27.4(7)$ GPa and $B' = 7.7(3)$. The relatively large B' value indicates a large change in compressibility with pressure. For phase II, we used a second-order BM EOS due to the limited number of data points, and the result was $V_0 = 79.3(5)$ Å^3 per formula and $B_0 = 73(3)$ GPa (B' fixed at 4). We expect strong structural connections between the phase I and phase II structures due to following observations: (1) most of the XRD peaks in phase

FIG. 4. (Color online) Rietveld refinement profiles for (a) phase I at 3.6 GPa and (b) phase II at 19.1 GPa.

I continuously evolve into phase II, (2) the volume drop from phase I to phase II is relatively small, and (3) the a of phase I splits into the a and c of phase II.

To fit the diffraction patterns of phase II, we tried a number of different structural models in the sesquioxides, such as c-As_2O_3, β-Sb_2O_3, γ-Sb_2O_3, β-Bi_2O_3 (similar to ϵ-Bi_2O_3), and m-As_2O_3 (claudetite), and the best fit came from the β-Bi_2O_3 structure. Figure 4 shows the Rietveld refinements for phase I and phase II. The inset of Fig. 4(b) shows the splitting of (002) and (222) in tetragonal structure that could not be described by a single reflection (400) in cubic structure. All of the Rietveld refinements were performed without adding preferred orientation. Table I shows the experimental crystallographic information for phase I and phase II from GSAS-EXPGUI. Table II shows the theoretical atomic positions that are electronically relaxed based on the experimental atomic positions (the lattices are fixed at the experimental values). Notice that the experimental and theoretical positions of Sb agree well with each other, while the O positions are slightly different. This is because O is a relatively weak x-ray scatter when compared to Sb, which then results in larger uncertainty in determining the atomic position of O during the Rietveld refinement.

In α-Sb_2O_3 phase I (from ambient to 15 GPa), the coordination of Sb-O increased from 3 to 6. As seen in Figs. 1(a) and 1(b), phase I changes from Sb_4O_6 cages (Sb-O_3 tetrahedra) at ambient pressure to a layered network (Sb-O_6 with three in-plane O and three out-of-plane O) at high pressure [20]. For phase II, the β-Bi_2O_3-type structure has two crystallographically inequivalent O sites: O1 links with two Sb at an angle close to $110°$ while O2 connects with two Sb almost linearly; for Sb, it forms Sb-O_5 pyramidlike polyhedra, where there are four in-plane O1 and one out-of-plane O2. Noticeably, in both phase I and phase II, the out-of-plane O atoms always stay on one side of the O plane, consistent with the fact that the lone $4s$ electron pair of Sb occupies the other side and does not form bonding with O. This further supports the role of the lone electron pair in determining local coordinations shown in previous calculations [19,41].

This phase II structure [Fig. 1(c)] bears some similarities to the previously reported γ-Sb_2O_3 structure [Fig. 1(d)]. In particular, the oxygen sites in γ-Sb_2O_3 can be approximated into two categories similar to those in Sb_2O_3 phase II. However, their structures differ in following aspects: (1) γ-Sb_2O_3 ($P2_12_12_1$, $Z = 8$) has a lower crystal symmetry than the tetragonal phase II (P-42_1c, $Z = 4$) phase and (2) γ-Sb_2O_3 has more crystallographically different Sb and O sites, e.g., six exact oxygen sites. These structural variations are strongly related to the different experimental conditions. γ-Sb_2O_3 was obtained at slightly lower pressure (9–11 GPa) and much higher temperature (300–500 °C). It is expectable that higher kinetic energies at elevated temperature may further break the bonding symmetry and increase local distortions.

Above 25 GPa, a sluggish amorphization was observed. For instance, the (211) of phase II at 2θ near 8.8° gradually became very broad while reflections (220) and (002) at near 9.5° became much weaker. At the highest pressure of 47.4 GPa in this study, the diffraction pattern [Fig. 2(b)] clearly shows a large amount of amorphous component.
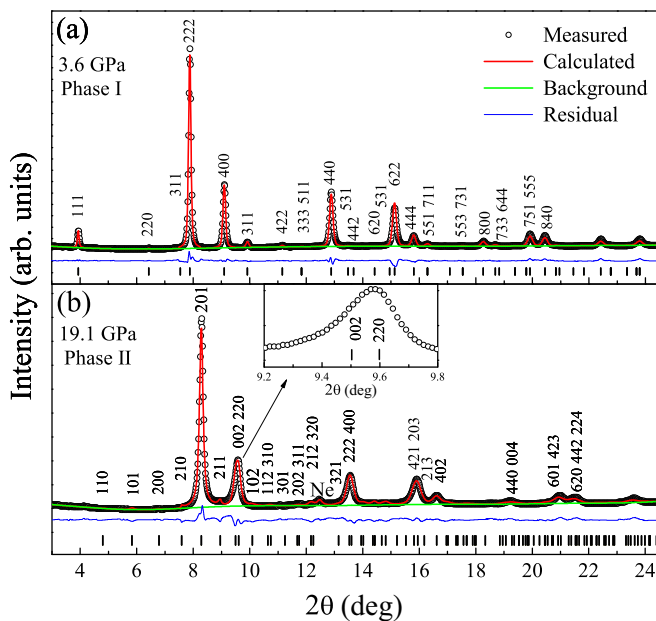
TABLE I. Experimental crystallographic information for phase I and phase II from GSAS-EXPGUI. Note that the atomic positions for *Fd*-3*m* come from Origin choice I.

Pressure (GPa)	Space group	Volume (Å^3)	Cell parameters		Experimental atomic positions			
			a (Å)	c (Å)	Atom	x	y	z
Phase I	Cubic	1383.5(1)	11.143(1)		Sb (32e)	0.885(1)	0.885(1)	0.885(1)
Ambient	*Fd*-3*m* (227)	$Z = 16$			O (48f)	0.179(1)	0	0
Phase I	Cubic	1141.6(1)	10.451(2)		Sb (32e)	0.877(1)	0.877(1)	0.877(1)
10.7 GPa	*Fd*-3*m* (227)	$Z = 16$			O (48f)	0.191(1)	0	0
Phase II	Tetragonal	267.9(1)	7.223(1)	5.135(2)	Sb (8e)	0.020(1)	0.257(1)	0.262(2)
17.2 GPa	*P*-42$_1$*c* (114)	$Z = 4$			O (8e)	0.342(4)	0.259(6)	0.442(5)
					O (4c)	0	0	0.324(12)

B. Raman spectroscopy measurements

To probe the changes of phonon modes during this structural transition and find proof for amorphization, we performed Raman experiments with a low laser power of 3 mW up to 48.6 GPa (Fig. 5). Although 3 mW is already very low, to rule out possible heating effects from the laser we repeated the Raman experiments with a much lower laser power of 1 mW up to 50.2 GPa and observed the same behavior.

Each Raman peak was fit to one Voigt function using PEAKFIT and the results are shown in Fig. 6. Below 15 GPa, our data agreed with the previous study that demonstrated the two isostructural transitions at ~3.5 GPa and 10 GPa [20], where the slopes of pressure dependence for some modes changed strongly, i.e., see the E_g mode in Fig. 6(d). Above 15 GPa, our study suggested the occurrence of a first-order structural transition due to following observations: (1) Between 15 and 30 GPa, the slopes of pressure dependence, i.e., the E_g mode ~120 cm^{-1}, shifted with pressure [see Fig. 6(d)], E_g mode ~300 cm^{-1} and F_2g modes ~360 cm^{-1} [see Fig. 6(c)] varied strongly. (2) At above 15 GPa, E_g mode ~125 cm^{-1} and A_1g mode ~275 cm^{-1} exhibited increasing full width half maximum (FWHM) with pressure. At above 30 GPa, obvious splitting of them could be observed [see Fig. 6(a)]. Linear extrapolations of these new peaks indicate that they may appear at ~20 and 30 GPa. Further increase in pressure resulted in strong decrease in peak intensities. At the highest pressure 48.6 GPa, no Raman peaks were observed.

C. Optical observations and first-principles calculations

Under pressure, the color of sample evolved from white to yellow, then to red, and finally to completely opaque, see Fig. 7, as were repetitively observed in all our experiments. Such dramatic changes suggest possible metallization and prompt us to investigate the electronic band structure and density of states (DOS). The DOS results from first-principles calculations at four representative pressures are shown in Fig. 8.

At ambient conditions, α-Sb_2O_3 is a semiconductor with an optical band gap of about 4 eV [4,5]. For ambient condition α-Sb_2O_3, our calculated indirect band gap is 3.0 eV, about 25% smaller than the experimental value, which is not surprising because first-principles calculations tend to underestimate the band gap. Visible light covers the range from violet (400 nm, 3.1 eV) to red (700 nm, 1.8 eV), so it is reasonable that the sample looked transparent to white light due to a lack of absorption in this region.

At 10.7 GPa, the band gap decreases to about 2.2 eV. Since visible light with higher energies will be largely absorbed, the sample would appear yellow. At higher pressure, phase II remains semiconducting with a much smaller band gap: 0.4 eV at 17.2 GPa and 0.2 eV at 21.8 GPa, which may explain why the color of the sample turned red and opaque finally. In contrast, the previous study assuming there was no first-order structural transition calculated the band gap to be as large as ~3.8 eV at 20 GPa, which would imply the sample being largely transparent to visible light [20]. At higher pressure, the featureless Raman spectra and total opacity we observed

TABLE II. Theoretical atomic positions for phase I and phase II from VASP. The cell parameters are fixed at the experimental values in Table I.

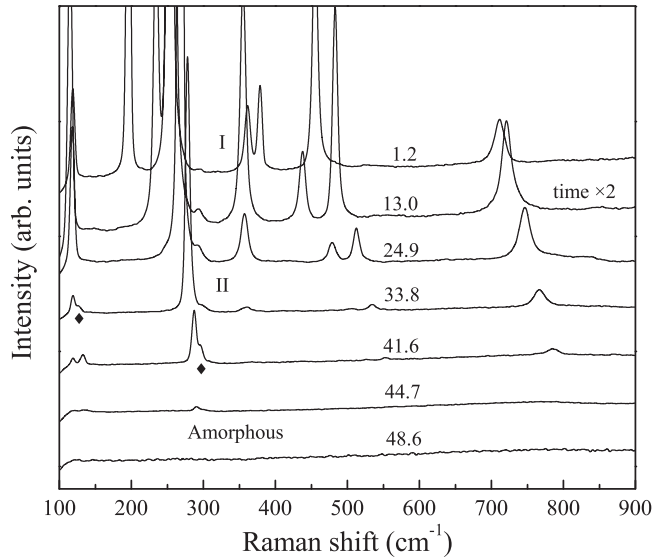| Pressure (GPa)	Space group	Volume (Å^3)	Cell parameters		Theoretical atomic positions			
			a (Å)	c (Å)	Atom	x	y	z
Phase I	Cubic	1383.5	11.143		Sb (32e)	0.883	0.883	0.883
Ambient	*Fd*-3*m* (227)	$Z = 16$			O (48f)	0.190	0	0
Phase I	Cubic	1141.6	10.451		Sb (32e)	0.874	0.874	0.874
10.7 GPa	*Fd*-3*m* (227)	$Z = 16$			O (48f)	0.199	0	0
Phase II	Tetragonal	267.9	7.223	5.135	Sb (8e)	0.023	0.267	0.245
17.2 GPa	*P*-42$_1$*c* (114)	$Z = 4$			O (8e)	0.310	0.230	0.518
					O (4c)	0	0	0.263

FIG. 5. Representative Raman spectra collected during compression. The diamond symbol indicates new peaks from phase II. The numbers represent pressures in unit of GPa.

at ~50 GPa suggest a possible metallic, amorphous phase of Sb_2O_3.

The band structures at four representative pressures, ambient pressure, 10.7, 17.2, and 21.8 GPa, are shown in Fig. 9. The results for phase I at ambient and 10.7 GPa, see Figs. 9(a) and 9(b), clearly shows the indirect feature of its electronic structure, where the indirect band gap lies in between Γ of the conduction band and L of the valence band. Remarkably, upon entering phase II [Fig. 9(c)], the band structure shows a direct feature. The direct band gap of phase II is located at Γ and this direct feature is well maintained upon further compression [Fig. 9(d)].

Our high-pressure study on α-Sb_2O_3 with neon as the pressure transmitting medium provides experimental evidence for transitions from the cubic phase I to a tetragonal phase II and eventually to an amorphous phase. It is noteworthy that one theoretical work has proposed a $\langle 100 \rangle$ Sb_2O_3 structure (equivalent to the phase II we identified) and showed that it was not dynamically stable without external pressure [19]. Here, we experimentally demonstrated that this structure can be stabilized under pressure. This further suggests that pressure can serve as an important tool in testing the theoretical models among various sesquioxide polymorphs.

Furthermore, the observation of hollow cavities (large ordered vacancies) in the crystalline phases further supports the role of the lone electron pair in the $\langle 111 \rangle$ and $\langle 100 \rangle$ vacancy arrays, as implied from previous calculations on defective fluorite models [19,41]. Phase I, composed of Sb_4O_6 cages, gradually transforms into a layered tetragonal phase II through local distortions and symmetry breaking, in which two crystallographically inequivalent O sites appeared. The physical properties (e.g., electric resistivity and optical conductivity) of these two phases are contrasting, resulting from a large reduction in the electronic band gap from a large-gap semiconductor (~4 eV, experimental) to a narrow-gap semiconductor (~0.5 eV, theoretical).
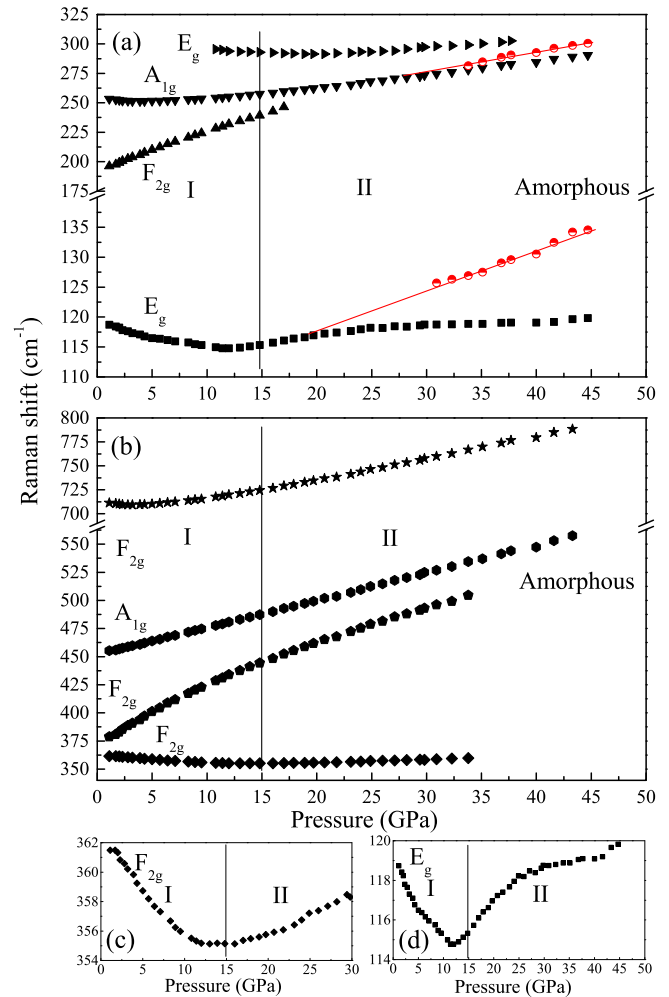

FIG. 6. (Color online) Evolution of Raman modes with pressure. Raman modes from (a) 110 to 325 cm^{-1} and (b) 325 to 800 cm^{-1}. New modes from phase II are marked by red and linearly extrapolated to lower pressures. Panels (c) and (d) show detailed changes of the F_{2g} and E_g modes.

Another topic worth discussion is the amorphization of late XV group sesquioxides [44,45,48,55]. Interestingly, the amorphous diffraction patterns we found at above 40 GPa [Fig. 2(a)] look similar to those of c-As_2O_3 at above 28 GPa [45] and the pattern for Sb_2O_3 glasses synthesized at ambient pressure [22].
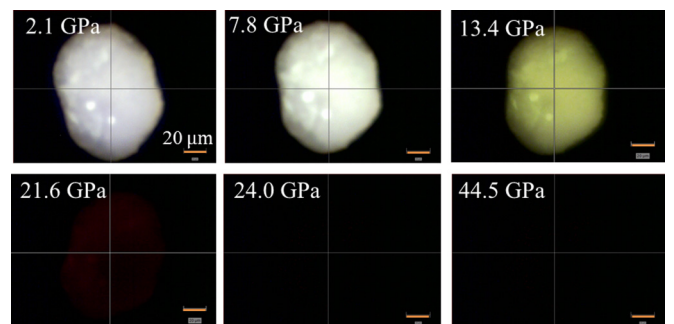

FIG. 7. (Color online) Optical photomicrographs of sample in transmitted light.
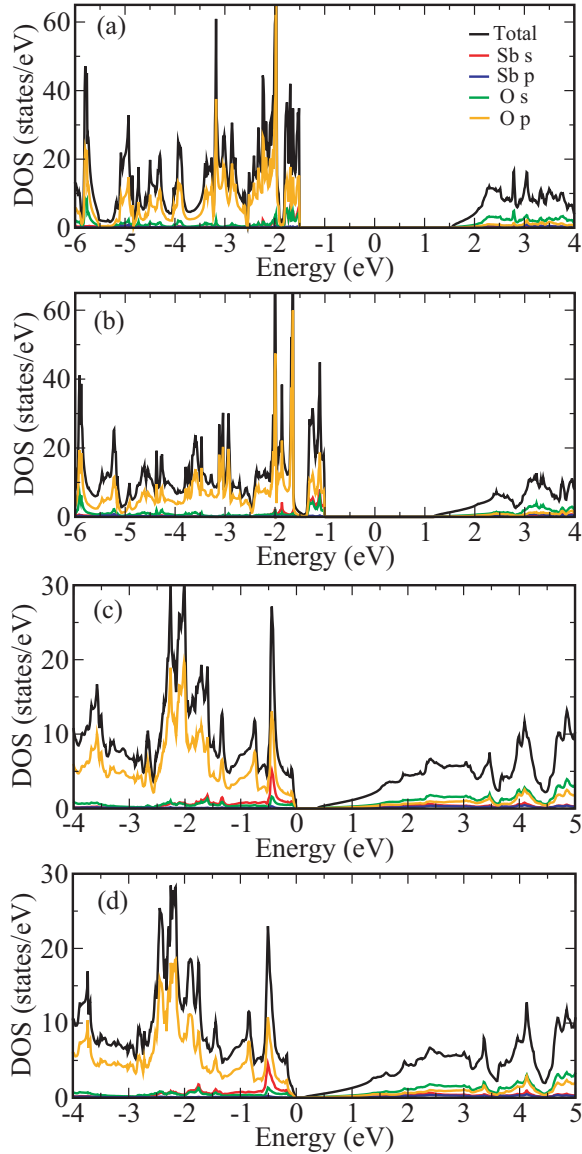
FIG. 8. (Color online) Calculated DOS of phase I at (a) ambient pressure and (b) 10.7 GPa, and phase II at (c) 17.2 GPa and (d) 21.8 GPa.

These patterns exhibited common features of a broad bump corresponding to the amorphous phase and a sharp peak at the large d spacing. α-Sb$_2$O$_3$ and c-As$_2$O$_3$ are isostructures built up by A_4O$_6$ (A = Sb and As) cages at ambient conditions. Under pressure, it is entirely possible that similar structural transition and amorphization mechanism exists in compressed α-Sb$_2$O$_3$ and c-As$_2$O$_3$. The Sb (As) coordination with nearby O in the amorphous phase may have a comparable coordination environment to those of phase II.

Among the late XV group sesquioxides, pressure-induced amorphization was also observed in α-Bi$_2$O$_3$ and β-Bi$_2$O$_3$ at high pressure [48,55], although their crystal structures are largely different from those of α-Sb$_2$O$_3$ and c-As$_2$O$_3$ at ambient conditions [48]. The widely observed sluggish amorphization process for both cagelike and layered late XV group sesquioxides [44,45,48,55] indicates an intriguing structural evolution from the long-range crystalline order to the
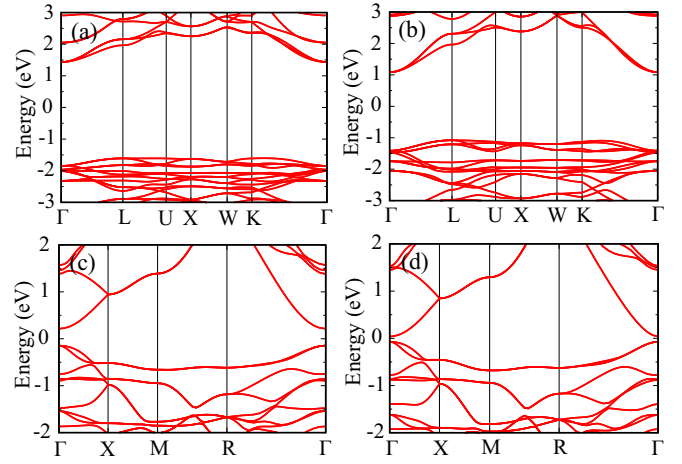

FIG. 9. (Color online) Calculated band structure of phase I at (a) ambient pressure and (b) 10.7 GPa, and phase II at (c) 17.2 GPa and (d) 21.8 GPa.

short-range amorphous order. Thermodynamic calculations and/or spectroscopic experiments are required to elucidate the underlying amorphization mechanism in late XV group sesquioxides. Also, the effect of pressure medium on the amorphization remains to be systematically explored.

IV. CONCLUSIONS

In summary, we investigated the high-pressure structural and electronic properties of α-Sb$_2$O$_3$ up to $\sim$50 GPa using neon as the pressure transmitting medium. The cubic phase I started to transform into a tetragonal phase II at $\sim$15 GPa. Besides from variations in local structures and crystal symmetries, these two phases have contrasting electronic properties, seen from the large differences of band gaps and dramatic changes in sample color and transparency. Higher pressure induces a sluggish amorphization process. Our results underscore high pressure as an important tool in exploring the connections between late XV group sesquioxides and understanding their amorphization mechanism.

[1] W. H. Zachariasen, J. Am. Chem. Soc. **54**, 3841 (1932).

[2] A. Byström, Nature (London) **167**, 780 (1951).

[3] O. Borgen and J. Krogh-Moe, Acta Chem. Scand. **10**, 265 (1956).

[4] C. Wood, B. Van Pelt, and A. Dwight, Phys. Status Solidi **54**, 701 (1972).

[5] B. Wolffing and Z. Hurych, Phys. Status Solidi **16**, K161 (1973).

[6] C. Svensson, Acta Crystallogr., Sect. B **30**, 458 (1974).

[7] C. Svensson, Acta Crystallogr., Sect. B **31**, 2016 (1975).

[8] P. S. Gopalakrishnan and H. Manohar, J. Solid State Chem. **15**, 61 (1975).

[9] C. A. Cody, L. DiCarlo, and R. K. Darlington, Inorg. Chem. **18**, 1572 (1979).

[10] P. J. Miller and C. A. Cody, Spectrochim. Acta, Part A **38**, 555 (1982).

[11] A. Datta, A. K. Giri, and D. Chakravorty, Phys. Rev. B **47**, 16242 (1993).

[12] J. S. Zabinski, M. S. Donley, and N. T. Mcdevittb, Wear **165**, 103 (1993).

[13] R. E. de Araujo, C. B. de Araujo, G. Poirier, M. Poulain, and Y. Messaddeq, Appl. Phys. Lett. **81**, 4694 (2002).

[14] J. H. Youk, R. P. Kambour, and W. J. MacKnight, Macromolecules **33**, 3594 (2000).

[15] A. J. G. Ellison and S. Sen, Phys. Rev. B **67**, 052203 (2003).

[16] S. J. Gilliam, J. O. Jensen, A. Banerjee, D. Zeroka, S. J. Kirkby, and C. N. Merrow, Spectrochim. Acta, Part A **60**, 425 (2004).

[17] H. Bryngelsson, J. Eskhult, L. Nyholm, M. Herranen, O. Alm, and K. Edstrm, Chem. Mater. **19**, 1170 (2007).

[18] A. Geng, L. Cao, C. Wan, and Y. Ma, Phys. Status Solidi C **8**, 1708 (2011).

[19] A. Matsumoto, Y. Koyama, A. Togo, M. Choi, and I. Tanaka, Phys. Rev. B **83**, 214110 (2011).

[20] A. L. J. Pereira, L. Gracia, D. Santamaria-Perez, R. Vilaplana, F. J. Manjón, D. Errandonea, M. Nalin, and A. Beltrán, Phys. Rev. B **85**, 174108 (2012).

[21] E. I. Voit, A. E. Panasenko, and L. A. Zemnukhova, J. Struct. Chem. **50**, 60 (2009).

[22] R. G. Orman, M.S. thesis, The University of Warwick, 2005.

[23] M. Nalin, Y. Messaddeq, S. J. L. Ribeiro, M. Poulain, V. Briois, G. Brunklaus, C. Rosenhahn, B. D. Mosel, and H. Eckert, J. Mater. Chem. **14**, 3398 (2004).

[24] M. Nalin, M. Poulain, M. Poulain, S. J. Ribeiro, and Y. Messaddeq, J. Nonklaus, C. Rosenhahn, B. D. Mosel, and H. Eckert, J. Non-Cryst. Solids **284**, 110 (2001).

[25] E. L. Falcao Filho, C. A. C. Bosco, G. S. Maciel, C. B. de Araujo, and L. H. Acioli, Appl. Phys. Lett. **83**, 1292 (2003).

[26] A. J. Frueh, Am. Mineral. **36**, 833 (1951).

[27] D. Ležal and K. Koňák, J. Non-Cryst. Solids **192–193**, 187 (1995).

[28] M. Drache, P. Roussel, and J.-P. Wignacourt, Chem. Rev. **107**, 80 (2007).

[29] N. M. Sammes and G. A. Tompsett, J. Eur. Ceram. Soc. **19**, 1801 (1999).

[30] D. Kristallstruktur, Z. Anorg. Allg. Chem. **318**, 1762 (1961).

[31] C. N. R. Rao, G. V. S. Rao, and S. Ramdas, J. Phys. Chem. **45**, 672 (1969).

[32] S. K. Blower and C. Greaves, Acta Crystallogr., Sect. C **44**, 587 (1988).

[33] A. F. Gualtieri, S. Immovilli, and M. Prudenziati, Powder Diffr. **12**, 90 (1997).

[34] D. Orosel, R. E. Dinnebier, V. A. Blatov, and M. Jansen, Acta Crystallogr., Sect. B **68**, 1 (2012).

[35] E. J. Roberts and F. Fenwick, J. Am. Chem. Soc. **50**, 2125 (1928).

[36] W. B. White, F. Dachille, and R. Roy, Z. Kristallogr. **125**, 450 (1967).

[37] K. E. Almin and A. Westgren, Ark. Kemi. Miner. Geol. **B22**, 15 (1944).

[38] I. R. Beatti, K. M. S. Livingsto, G. A. Ozin, and D. J. Reynolds, J. Chem. Soc. A **3**, 449 (1970).

[39] P. Ballirano and A. Maras, Z. Kristallogr. NCS **217**, 177 (2002).

[40] N. Cornei, N. Tancret, F. Abraham, and O. Mentr, Inorg. Chem. **45**, 4886 (2006).

[41] A. Matsumoto, Y. Koyama, and I. Tanaka, Phys. Rev. B **81**, 094117 (2010).

[42] E. M. Levin and R. S. Roth, J. Res. Natl. Bur. Stand., Sect. A **68A**, 197 (1964).

[43] A. Grzechnik, J. Solid State Chem. **144**, 416 (1999).

[44] C. Chouinard and S. Desgreniers, Solid State Commun. **113**, 125 (1999).

[45] E. Soignard, S. A. Amin, Q. Mei, C. J. Benmore, and J. L. Yarger, Phys. Rev. B **77**, 144113 (2008).

[46] S. Ghedia, T. Locherer, R. Dinnebier, D. L. V. K. Prasad, U. Wedig, M. Jansen, and A. Senyshyn, Phys. Rev. B **82**, 024106 (2010).

[47] T. Locherer, D. L. V. K. Prasad, R. Dinnebier, U. Wedig, M. Jansen, G. Garbarino, and T. Hansen, Phys. Rev. B **83**, 214102 (2011).

[48] A. L. J. Pereira, D. Errandonea, A. Beltrn, L. Gracia, O. Gomis, J. A. Sans, B. Garc-a-Domene, A. Miquel-Veyrat, F. J. Manjón, A. Muñoz, and C. Popescu, J. Phys.: Condens. Matter **25**, 475402 (2013).

[49] B. H. Toby, J. Appl. Crystallogr. **34**, 210 (2001).

[50] G. Kresse and D. Joubert, Phys. Rev. B **59**, 1758 (1999).

[51] G. Kresse and J. Hafner, Phys. Rev. B **47**, 558(R) (1993).

[52] J. P. Perdew, K. Burke, and M. Ernzerhof, Phys. Rev. Lett. **77**, 3865 (1996).

[53] P. Hohenberg and W. Kohn, Phys. Rev. **136**, B864 (1964).

[54] P. E. Blöchl, Phys. Rev. B **50**, 17953 (1994).

[55] A. L. J. Pereira, R. V. J. A. Sans, O. Gomis, F. J. Manjn, P. Rodrguez-Hernndez, A. Muoz, C. Popescu, and A. Beltrn, J. Phys. Chem. C **118**, 23189 (2014).